CHINESE JOURNAL OF PHYSICS VOL. 54, NO. 1 February 2016

Electronic Structure, Mechanical and Optical Properties of $TiAl_3$ ($L1_2$ & $D0_{22}$) via First-Principles Calculations

Altaf Hussain,[1,*] Salman Mehmood,[1] Nasir Rasool,[1]
Neng Li,[2] and C. C. Dharmawardhana[3]

[1]*Department of Physics, The Islamia University of Bahawalpur, Bahawalpur, Punjab 63100, Pakistan*
[2]*Center for Photovoltaics and Solar Energy, Shenzhen Institutes of Advanced Technology, Chinese Academy of Sciences, Shenzhen 518055, PR China*
[3]*Department of Physics and Astronomy, University of Missouri—Kansas City, Kansas City, MO 64110, USA*

(Received July 10, 2015; Revised November 2, 2015)

Density functional theory based *ab initio* calculations have been performed to study the electronic structure, mechanical and optical properties of $L1_2$ and $D0_{22}$ phases in $TiAl_3$ intermetallic alloy system. For electronic structures, bonding, and optical properties calculations we used orthogonalized linear combination of atomic orbitals (OLCAO) method, while for mechanical properties, Vienna *ab initio* simulation package (VASP) is used. The band structure calculations show same number of bands crossing the Fermi level in both the $L1_2$ and $D0_{22}$ phases. Total density of states (TDOS) spectra reveal that the bottom of conduction band is dominated by Ti, while top of valence band being contributed mostly by Al atoms in both the phases. In $D0_{22}$ phase, DOS at the Fermi level $N(E_F)$ are 5.51 while in $L1_2$ phase are 4.67 states/eV formula unit. Localization index calculations reveal that there exist highly localized states above the Fermi level. Results of elastic stiffness constants and bulk mechanical properties are in good agreement with the reported experimental data in literature for both the phases. Optical conductivity spectra in both the phases are rich in structures with the most prominent peak existing at 4.80 eV.

DOI: PACS numbers: 31.10.+z, 31.15.es, 34.70.+e

I. INTRODUCTION

Intermetallics are a unique class of materials having characteristics of both metals and ceramics. They differ from conventional metal alloys by possessing long-range-order. Highly directional covalent and ionic bonds dominate in ceramics, while in metals, the unique deformation properties result from non-directional metallic bonding. Intermetallics contain both metallic and covalent type bonds, depending on the constituent metals. Mixed bonding feature in intermetallics provides mechanical properties that are between metals and ceramics. Strength at high-temperature and superior oxidation resistance make intermetallic materials exceptional candidates for high-temperature applications. Other promi-

*Electronic address: altafiub@yahoo.com

nent advantages are longer service life, efficient operation at high-temperature and reliable performance [1–3].

"*Intermetallic compounds*" are considered to be perfectly ordered stoichiometric alloys with specific formulas. However, the term "*intermetallic alloy*" refers to partly ordered stoichiometric alloys and to ordered non-stoichiometric alloys. Titanium based alloys have been widely used over the past many decades in industry due to their high specific strength, good corrosion resistance as well as high thermal stability [4, 5]. The structures and properties of Ti-Al ordered intermetallic alloys were studied extensively over the past by many research groups, and as a result of these efforts many attractive properties were identified and characterized [4–6]. The systematic science of alloys (SSA) [7, 8] framework shows that the Ti-Al system includes FCC, HCP, and BCC lattice systems, besides having a liquid system. The Ti-Al FCC lattice system may have some ordered intermetallic FCC $Ti_xAl_{(1-x)}$ alloy systems with Ti_3Al, Ti_2Al, TiAl, $TiAl_2$, and $TiAl_3$ types. The ordered intermetallic FCC $TiAl_3$-type alloys may be observed to be found in $D0_{22}$ and $L1_2$ phases, and other intermetallic compounds as well as their corresponding ordered intermetallic $Ti_xAl_{(1-_x)}$ alloys [9, 10]. Low density and high melting point make $TiAl_3$ compounds a good candidate as metal matrix composites [11].

Through literature survey, we reach although a number of theoretical and experimental studies have been performed on $TiAl_3$ intermetallic alloy system, yet there exists a quest for detailed information about electronic structure, mechanical and optical properties of this system. In current study, our focus is to provide a detailed picture of electronic structure, mechanical, and optical properties of the two stoichiometric phases, $D0_{22}$ and $L1_2$ in $TiAl_3$ intermetallic alloy system. All calculations on electronic structure, bonding, and optical properties are performed using density functional theory (DFT) based orthogonalized linear combination of atomic orbitals (OLCAO) method [12, 13]. The OLCAO method uses localized atomic orbitals expanded in Gaussian type wave functions as the basis set for the wave function expansion. More details on OLCAO will be provided in Section III. For structure relaxation and mechanical properties calculations we used VASP [14, 15]. The combination of these two methods is well suited for large complex systems and its successful application to many material systems has been fully demonstrated [16, 17]. The paper is organized as follows: in the following Section II, we briefly review the two structures $D0_{22}$ and $L1_2$, Section III describes the method of calculation and in Section IV, we discuss the results of the electronic structures, bonding, mechanical and optical properties. Finally in Section V, we present a summary and some conclusions of this study.

II. STRUCTURE DESCRIPTION

$TiAl_3$ intermetallic alloy system is observed to exist as a simple cubic $CuAu_3$ structure. Ti atoms occupy the corner positions of the cube, while Al atoms lie at the face centered positions. Figure 1 (a) shows the $L1_2$ FCC phase of $TiAl_3$ system. Figure 1 (b) represents the simplest one Dimensional-Long Period Structure (1D-LPS) of $D0_{22}$ tetragonal structure constructed, based on $L1_2$ unit cell. The $D0_{22}$ unit cell consists of two $L1_2$

cubes stacked along the z direction, with an anti-phase shift between every cube.

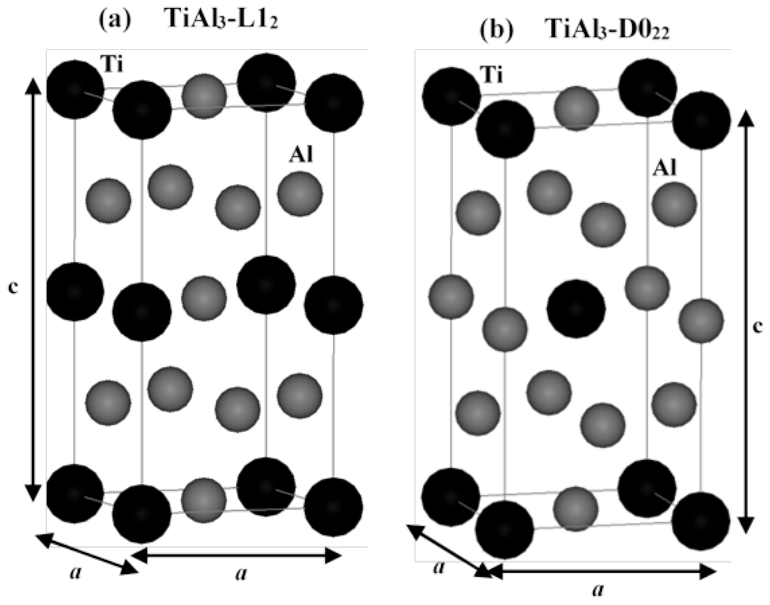

FIG. 1: Crystal structures of the two phases (a) $L1_2$ and (b) $D0_{22}$ in $TiAl_3$ intermetallic alloy system. Dark black circles represent Ti atoms, while grey circles stand for Al atoms.

Among the long period super lattice structures of $TiAl_3$ intermetallic alloy system, $L1_2$ and $D0_{22}$ have been studied in this research. Without considering the influence of the second nearest-neighbor atoms, the $D0_{22}$ and $L1_2$-$TiAl_3$ compounds have the same structural parameters and the same properties. It means that the difference in their structural parameters and properties should be credited to the different second-neighbor configuration.

III. METHODOLOGY

To calculate electronic structure, inter-atomic bonding, and optical properties of $L1_2$ and $D0_{22}$ phases in $TiAl_3$ intermetallic alloy system we used the first-principles based OLCAO method [12, 13]. OLCAO is based on the local density approximation (LDA) of DFT [18, 19]. This method has already been used successfully to study both crystalline [17, 20] and non-crystalline systems [21, 22]. Three types of basis sets are normally used in the OLCAO calculations. The full basis (FB) set consists of the core orbitals, occupied valence orbitals, and the next empty shell of unoccupied orbitals for each atom. FB is used for the determination of the self-consistent potential and subsequent calculations of band structures and density of states (DOS). For $TiAl_3$ system, the FB has atomic orbitals of Ti-($1s$, $2s$, $2p$, $3s$, $3p$, $3d$, $4s$, $4p$, $4d$, $5s$, and $5p$), and Al-($1s$, $2s$, $2p$, $3s$, $3p$, $3d$, $4s$, and $4p$).

For optical properties calculation, an extended basis (EB) set is used, which includes one additional shell of empty orbitals. These orbitals improve the accuracy of the higher states in the conduction band. For effective charge (Q^*) and bond order (BO) calculations using Mulliken analysis [23], the minimal basis (MB) set is used which provides more localized basis. Total energy convergence is set at 0.0001 a.u. energy difference. To attain high accuracy sufficient k-points sampling are used, which are listed in Table I along with the crystal structure data.

TABLE I: Crystal structure data used in present study.

	$L1_2$	$D0_{22}$
Crystal type	Cubic	Tetragonal
Space group (no.)	$Pm\bar{3}m$ (221)	$I4/mmm$ (139)
Lattice parameters		
a (Å)	3.97210	4.003
b (Å)	3.97210	4.003
c (Å)	7.94420	8.005
α	90.000°	90.000°
β	90.000°	90.000°
γ	90.000°	90.000°
Atoms/unit cell	8	8
Atom types (no. of atoms of different type)		
Ti	1	1
Al	1	2
Non-equivalent sites	2	3
scf k-points	185	196
OLCAO k-points	185	405

In addition to the usual band structure and density of states (DOS) calculations, the quantitative evaluation of the effective charge Q^* at each atom site is crucial in OLCAO method. The effective charge Q^*_α, is defined as the calculated valence electrons associated with an atom α in the crystal which can provide information about charge transfer (gain or loss of electronic charge from the neutral atom). It is defined as:

$$Q^*_\alpha = \sum_i \sum_{n,occ} \sum_{j,\beta} C^{*n}_{i\alpha} C^n_{j\beta} S_{i\alpha,j\beta}, \tag{1}$$

where $C^n_{j\beta}$ are the eigenvector coefficients, n is the band index and j and β are orbital and atomic labels respectively.

Bond order (BO) provides a notion about the relative strength of a bond between a pair of atoms. It is considered to carry information about the microscopic origin for the mechanical properties. BO is calculated as follows

$$\rho_{\alpha\beta} = \sum_{n,occ} \sum_{i,j} C^{*n}_{i\alpha} C^{n}_{j\beta} S_{i\alpha,j\beta}. \tag{2}$$

In this equation $\rho_{\alpha\beta}$ denotes the bond order for the atom pair (α, β), n is the band index, i and j are the orbital quantum numbers, and the C are the eigenvector coefficients of the Bloch function $b(\vec{k}, \vec{r})$.

Distribution of electronic charge around each atom of a particular system (crystal or glass) is approximated by localization index (LI). The LI for the state n with energy E_n is defined as:

$$L(E_n) = \left[\sum_{\alpha=1}^{N} (\rho^n_\alpha)^2 \right]^{1/2} \tag{3}$$

where ρ^n_α is the fractional electron charge assigned to the α^{th} atom according to Mulliken's prescription [24] and calculated from the resulting Eigen functions. For amorphous systems the localization of states is typically encountered near band edges in accordance with the Anderson model [25].

Elastic stiffness constants are critical for assessing how a solid responds under applied strain within the elastic limit. The elastic tensor enables the evaluation of bulk mechanical properties. In the present study, we use the strain-stress analysis approach [26]. In this approach, a small strain of plus or minus 1% is applied to each independent strain element in the fully relaxed structure. The elastic coefficients C_{ij} are calculated by solving a set of linear equations:

$$\sigma_{ij} = \sum_{ij} C_{ij} \varepsilon_j. \tag{4}$$

From the calculated C_{ij} values, one can obtain bulk mechanical properties (bulk modulus K, shear modulus G, Young's modulus E, and Poisson's ratio η) using the well-known Voight-Reuss-Hill scheme [27, 28].

For optical properties calculation, we start with the imaginary component of the complex dielectric function $\varepsilon(\hbar\omega) = \varepsilon_1(\hbar\omega) + i\varepsilon_2(\hbar\omega)$ for interband optical transitions in the random phase approximation (RPA) according to:

$$\begin{aligned} \varepsilon_2(\hbar\omega) \;=\; & \left(\frac{e^2}{\pi m E \omega} \right) \int d\vec{k} \sum_{n,l} \left| \left\langle \Psi_n \left(\vec{k}, \vec{r} \right) \right| \vec{P} \left| \Psi_l \left(\vec{k}, \vec{r} \right) \right\rangle \right|^2 f_l \left(\vec{k} \right) \\ & \times \left[1 - f_n \left(\vec{k} \right) \right] \delta \left[E_n \left(\vec{k} \right) - E_l \left(\vec{k} \right) - E \right] \end{aligned} \tag{5}$$

where $E = \hbar\omega$ is the photon energy, $f(\vec{k})$ is the Fermi distribution function, l labels an occupied state and n an unoccupied state, and $\Psi_n(\vec{k}, \vec{r})$ is the Bloch wave function for the

n^{th} band with energy $E_n(\vec{k})$ at Brillouin zone point k. The momentum matrix element (MME) $\langle \Psi_n(\vec{k},\vec{r})|\vec{P}|\Psi_l(\vec{k},\vec{r})\rangle$ was explicitly calculated from the *ab initio* wave functions. The real part of the dielectric function $\varepsilon_1(\hbar\omega)$ is then obtained from the imaginary part $\varepsilon_2(\hbar\omega)$ using the Kramers-Kronig transformation.

IV. RESULTS AND DISCUSSION

IV-1. Electronic Structure

Band structure derives from the dynamical theory of diffraction of the quantum mechanical electron waves in a periodic crystal lattice with a specific crystal system and Bravais lattice. The band structure calculation gives the most direct comparison with experiments and is the plot of energy eigenvalues of the system at special k-points in reciprocal space. The k-points are chosen specifically within the irreducible portion of the Brillion zone. A material can be classified as metal, semi-metal, half-metal, semiconductor or an insulator by observing this type of plot. Figure 2 shows the calculated band structures of $L1_2$ and $D0_{22}$ phases in $TiAl_3$ alloy system along high symmetry directions. Fermi level (E_F) is set at 0 eV energy value (the solid horizontal line in the plots a and b of Figure 2). It is observed that band structure of $L1_2$ phase is more complex and carries more structures than $D0_{22}$ phase. However, the same number of bands cross the Fermi level (4 bands) in both the $L1_2$ and $D0_{22}$ phases. The band structures show no gap at Fermi level which confirms the conducting nature of the two phases.

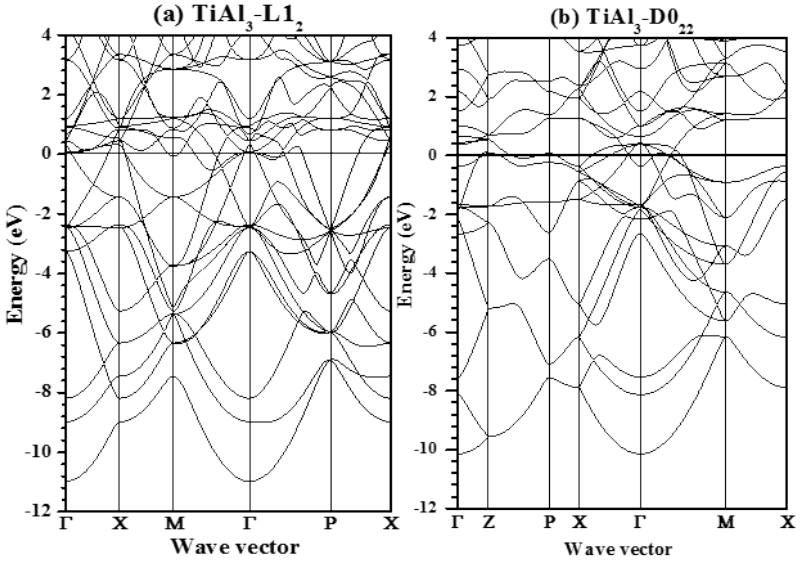

FIG. 2: Band structures along high-symmetry lines of the two phases (a) $L1_2$ and (b) $D0_{22}$ in $TiAl_3$ intermetallic alloy system. The solid horizontal line represents the Fermi level ($E_F = 0$ eV).

The total density of states (TDOS) spectrum represents number of available states

per energy interval. For crystalline systems in general, the TDOS can be observed to have a number of different peak structures at various points both above and below the highest occupied energy level which is known as Fermi level in metals. The partial density of states (PDOS) break down the TDOS into contributions from either elements of desire or their orbital of interest in order to understand the bonding. The energy differences between various peaks also assist in analyzing specific structures of the optical spectra. The calculated TDOS and atom-resolved PDOS spectra of $L1_2$ and $D0_{22}$ phases in $TiAl_3$ intermetallic alloy system are shown in Figure 3 (a) and (b), respectively. In the TDOS spectrum of $L1_2$ phase (Figure 3 (a)), we observe the highest peak at 0.96 eV above the Fermi level which spawns from the Ti sites. The top of valence band (TVB) also carries a peak at -2.27 eV which is clearly coming from Al sites. In the conduction band (CB) region of TDOS spectrum of $L1_2$ phase, we observe two more peaks at 2.63 and 5.94 eV. The first peak finds roots in Ti sites, while the other one in Al sites. There also exists a shoulder like structure at 0.28 eV originating from Ti in the TDOS spectrum. The Fermi level seems to cut the steep side of the TDOS spectrum in both the phases. The TDOS spectrum of $D0_{22}$ phase (Figure 3 (b)) is different from the $L1_2$ phase. There are two non-equivalent Al sites, Al1 and Al2 in $D0_{22}$ phase, while $L1_2$ phase has one Al site. The highest peak (at 1.48 eV) in CB in $D0_{22}$ phase comes from Ti sites similar to $L1_2$ phase. The total number of states at Fermi level are 4.67 and 5.51 states/(eV formula unit) in $L1_2$ and $D0_{22}$ phases respectively following primitive cell calculations. Large value of $N(E_F)$ in case of $D0_{22}$ phase is consistent with the band structure diagram in Figure 2 (b).

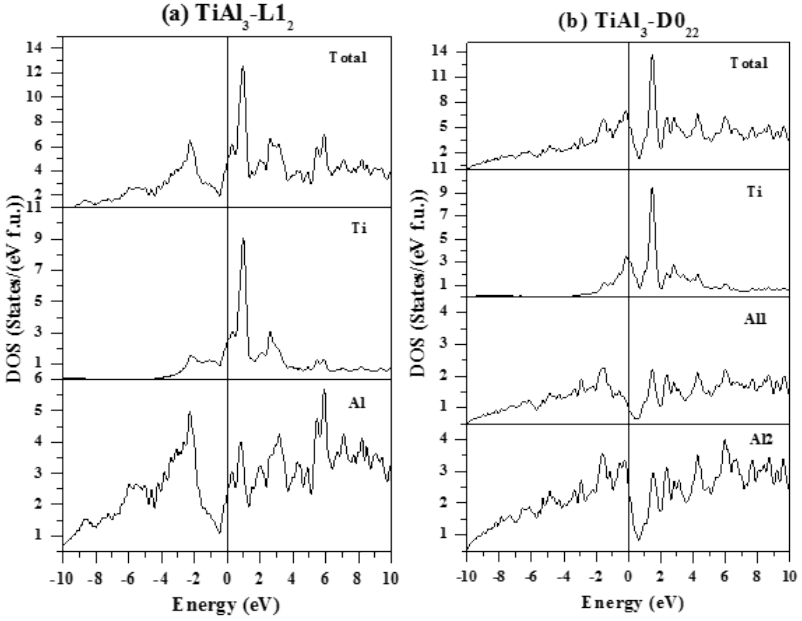

FIG. 3: Total and element resolved partial DOS plots of the two phases (a) $L1_2$ and (b) $D0_{22}$ in $TiAl_3$ intermetallic alloy system.

To further analyze electronic structure, we decompose the TDOS spectra of individual elements into the orbital resolved PDOS spectra. Figure 4 (a) and (b) shows the orbital resolved PDOS along with the Ti/Al TDOS spectra of $L1_2$ and $D0_{22}$ phases in $TiAl_3$ respectively. We observe that Ti TDOS spectra are contributed by $3d$ states in both the phases. The Al TDOS spectra are contributed by $3s$, $3p$ and $3d$ orbitals in the two phases. The main peak observed (at $-2.25/-1.61$ eV in $L1_2/D0_{22}$) in Al TDOS spectra below the Fermi level comes from Al-$3p$ states. The states at the Fermi level are contributed by Al-$3p$ and $3d$ orbitals. Al $3s$ orbitals have negligible contribution to the states at the Fermi level. We see that the lower part of the VB in Al TDOS spectra in both the phases comes from Al $3s$ orbitals.

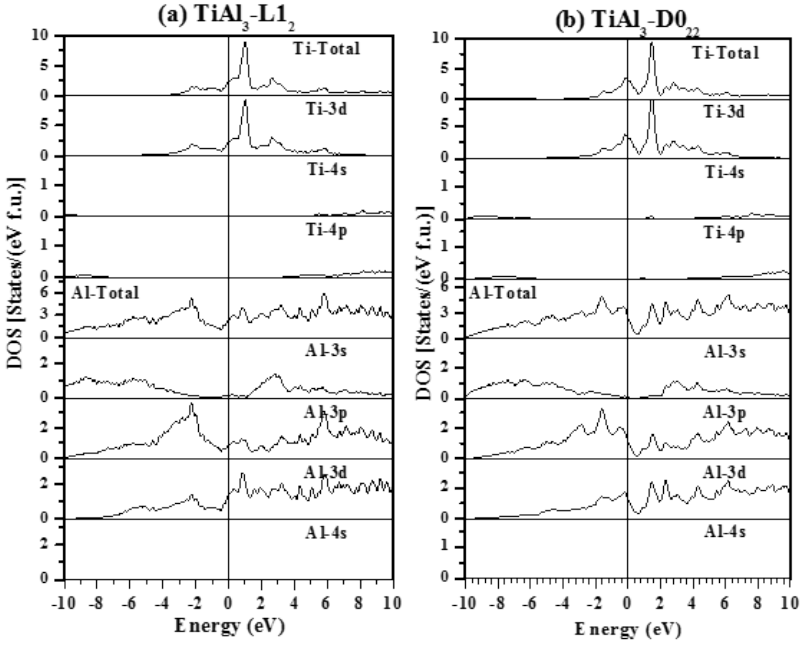

FIG. 4: Total and orbital resolved partial DOS plots of the two phases (a) $L1_2$ and (b) $D0_{22}$ in $TiAl_3$ intermetallic alloy system.

Effective charge (Q^*) is a static representation of the charge distribution on ground state and provides the chemical nature of the material system under consideration. The calculated Q^* data of $TiAl_3$ intermetallic alloy system for both $L1_2$ and $D0_{22}$ phases is listed in Table II. Effective charge calculation depicts much of microscopic information about the electronic structure of material. In $L1_2$ phase the Q^* value for Ti remains constant at 3.936 electrons/atom, while Al ranges from 2.941 to 3.116 electrons/atom. These results show a net charge loss on Ti atoms and gain on Al atoms, which is consistent with the chemical nature of Ti and Al. The average Q^* values observed by Ti and Al in $L1_2$ phase are 3.936 and 3.022 electrons/atom respectively. This indicates a considerable charge transfer from Ti to Al. Ti loses a net charge of 0.064 electrons/atom on average, while the Al atoms gain

an average of 0.022 electrons/atom. In $D0_{22}$ phase the Q^* value of Ti also remains constant as in $L1_2$ phase but at slightly higher value of 4.082 electrons/atom. Q^* value of Al varies from 2.886 to 3.017 electrons/atom. The average Q^* values observed by Ti and Al in $D0_{22}$ phase are 4.082 and 2.973 electrons/atom respectively. From these average Q^* values we observe a reverse charge transfer trend (Ti atoms gain charge while Al atoms lose) in $D0_{22}$ phase to $L1_2$ phase. These data indicate a considerable charge transfer from Al to Ti. Ti atoms gain a net charge of 0.082 electrons/atom on average, while the Al atoms lose an average of 0.027 electrons/atom in $D0_{22}$ phase.

TABLE II: Effective Charge Q^* (electrons/atom) in $L1_2$ and $D0_{22}$ Phases of $TiAl_3$ Intermetallic Alloy.

Phase	Element	$Q^*_{\min}$	$Q^*_{\max}$	Q^*_{ave}	ΔQ^*
$L1_2$	Ti	3.936	3.936	3.936	−0.064
	Al	2.941	3.116	3.022	+0.022
$D0_{22}$	Ti	4.082	4.082	4.082	+0.082
	Al	2.886	3.017	2.973	−0.027

Crystal stiffness and cohesion is usually judged through bond order calculations. It is observed that bond orders totality depends on the number of bonds and the strength of each bond. Table III lists the major results on BO calculations, including total BO (TBO) values and the bond order density (BOD) values of both the $L1_2$ and $D0_{22}$ phases of $TiAl_3$ intermetallic alloy system. BOD is defined as the total bond order per unit volume. For example, $L1_2$ (primitive cell) has 52.8% of its total BO values from Ti-Al bonds and 47.2% from Al-Al bonds. Thus, the Ti-Al bonds are the dominant contributor and play major role in the overall stiffness in $TiAl_3$ alloy system. $D0_{22}$ phase follows the same trends of domination of Ti-Al bonds.

TABLE III: Summary of bond order for each type of bond (BO%).

Phase	Bond type	TBO (BO%)	BOD	TBOD
$L1_2$	Al-Al	1.19 (47.16%)	0.0190	0.0403
	Ti-Al	1.34 (52.83%)	0.0213	
$D0_{22}$	Al-Al	2.20 (42.18%)	0.0172	0.0407
	Ti-Al	3.02 (57.81%)	0.0235	

Figure 5 (a) and (b) shows the calculated results on LI of $L1_2$ and $D0_{22}$ phases respectively. These results have been calculated using supercell approach in the energy range of −10 to 10 eV. We used $4 \times 4 \times 4$ and $4 \times 4 \times 2$ supercell models with 256 atoms for $L1_2$ and $D0_{22}$ phases respectively. It is generally considered that the states are usually

localized at the band edges than those at the center of the bands in disordered amorphous solids. This rule may not strictly apply in metallic systems due to the presence of delocalized electron clouds. Moreover it is observed that s- or p-orbitals are usually less localized than d-orbitals. In current study, our focus is to explore the region of few eV range above and below the Fermi level. In this region usually the Ti-3d states play major role. We observe that states near E_F are more localized in both $L1_2$ and $D0_{22}$ phases. Ti d-orbitals of the type xx, yy, zz, x^2-y^2, r^2-3z^2 are responsible for this behavior. Some of these orbitals are more localized than others. Within about 1.31 eV of the Fermi level, there is dramatic increase in the LI of states in $L1_2$ phase. Only the states dominated by d-orbitals show this type of behavior. On the other hand, we see that the states are completely delocalized above 3 eV. This is obvious in the sense that they comprise of s- and p- orbitals. Below the E_F there are few localized states observed within 0 to -2 eV. The trend is slightly different in the case of $D0_{22}$ phase. The LI of the states below 1.70 eV sharply increases. The states above 4 eV are completely delocalized in $D0_{22}$ phase. We are unable to observe any localized states below the E_F in $D0_{22}$ phase.

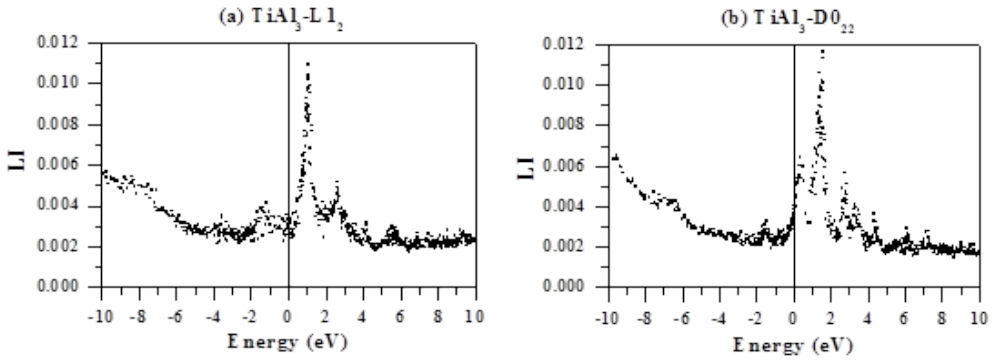

FIG. 5: Localization index (LI) plots of the states of the two phases (a) $L1_2$ and (b) $D0_{22}$ of $TiAl_3$ intermetallic alloy system.

IV-2. Mechanical Properties

Exploration of the elastic and mechanical behaviors of technologically related class of materials opens their new ways of applications. To assess the behavior of a particular solid material under applied strain, knowledge of its elastic stiffness constants is quite critical. In the present study for elastic properties calculation of $L1_2$ and $D0_{22}$ phases of $TiAl_3$ alloy system, we use the strain-stress analysis approach. Our calculated elastic stiffness constants for $L1_2$ and $D0_{22}$ phases are listed in Table IV. These results reveal diverse elastic behavior of the two $TiAl_3$ phases. Due to cubic symmetry, $L1_2$ phase has three independent tensor coefficients: C_{11}, C_{44}, and C_{12}. On the other hand, $D0_{22}$ phase has six independent tensor coefficients: C_{11}, C_{33}, C_{44}, C_{66}, C_{12}, and C_{13} due to tetragonal symmetry. Detailed analysis

of the data shows that C_{11} value in $D0_{22}$ phase is 2.6% higher than $L1_2$ phase. On the other hand, the value of shear constant C_{44} is more than double (79.8% higher) for $D0_{22}$ phase as compared to $L1_2$ phase. The off diagonal constant C_{12} is 36.5% higher in $D0_{22}$ phase. This analysis reveals that $L1_2$ phase is relatively weaker as compared to $D0_{22}$ phase.

TABLE IV: Calculated Elastic Constants and Bulk Mechanical Properties using Voigt-Reuss-Hill Approximation (VRH).

Phase	Applied strain									
	C_{11} (GPa)	C_{33} (GPa)	C_{44} (GPa)	C_{66} (GPa)	C_{12} (GPa)	C_{13} (GPa)	K (GPa)	G (GPa)	E (GPa)	η
$L1_2$	191.69		49.13		64.61		106.96	54.46	139.68	0.28
							91.8[a]	72.1[a]	171.5[a]	0.19[a]
							97.0[a]	73.9[a]	176.9[a]	0.20[a]
							102.5[a]	67.2[a]	165.5[a]	0.23[a]
$D0_{22}$	196.61	222.35	88.31	124.33	88.20	44.70	107.70	86.33	204.38	0.18
	217.7[b]	217.5[b]	92.0[b]	116.5[b]	57.7[b]	45.5[b]	105.6[b]	93.0[b]	215.7[b]	0.16[b]

[a] [29]
[b] [30]

We observe that C_{33} value is reasonably larger than C_{11} in $D0_{22}$ phase, which indicates that the structure is stiffer along the crystallographic c-axis. Similarly, the value of shear stiffness constant C_{66} is distinctively larger than C_{44}. This can be explained by viewing the atomic structure of the $D0_{22}$ phase. The atomic arrangement in the (001) plane seems more rigid than along (100) or (010) planes. Among the off diagonal elastic coefficients C_{12} is larger than C_{13}. The larger value of C_{12} implies that the atomic configuration and bonding in the directions [100] and [010] are more strongly interrelated than in C_{13}. Nakamura *et al.* [30] have measured the elastic constants of $TiAl_3$ ($D0_{22}$ phase) single crystals. Their results have been presented in Table IV along with our calculations on the $L1_2$ and $D0_{22}$ phases for a nice comparison. All the calculated elastic stiffness constants except C_{12} show reasonably good agreement with the experimentally measured results.

From the calculated elastic stiffness coefficients, we can obtain their bulk mechanical properties: bulk modulus (K), shear modulus (G), Young's modulus (E), and Poisson's ratio (η) which are also listed in Table IV together with the experimental data from literature [29, 30]. On comparison with the experimental data for $L1_2$ phase [29], we see that there exists a good agreement. However, the experimental data from Ref. [29] shows larger deviation from our results, which could be due to the different values of longitudinal and shear wave speeds employed to measure these results on bulk mechanical properties. On the other hand, for $D0_{22}$ phase, we observe a nice agreement with the experimentally measured

data by Nakamura *et al.* [30]. Finally we see that these calculations reveal that all the three moduli (K, G, and E) are larger in $D0_{22}$ phase as compared to $L1_2$ phase, consistent with the elastic stiffness coefficients results. However, the Poisson's ratio exhibits reverse behavior.

IV-3. Optical Properties

The imaginary part (ε_2) of linear dielectric function (LDF) for $L1_2$ and $D0_{22}$ phases of $TiAl_3$ alloy is calculated in the energy range of 0 to 10 eV using supercell approach and presented in Figure 6 (a) and (b), respectively. The ε_2 curve in $L1_2$ phase shows numerous spectral features. There is a kink A present at 0.44 eV and a plateau region in the energy range of 1.75 – 5.05 eV. Just before the plateau, there is a small valley like feature observed at point C. Within the given plateau range, the ε_2 spectrum observes two less prominent peaks B and D at 2 and 4.79 eV respectively. In between these two peaks (B and D), some small bump like features are also present. From point D at 4.79 eV, the curve shows a decrement in its value. There is also a shoulder E present at 1.02 eV before valley C. The curve ascends sharply for the energy values below 0.32 eV. No other interesting feature is observed above energy value of 6.50 eV. ε_2 spectrum of $D0_{22}$ phase is different from $L1_2$ phase. The kink like structure A observed at 0.44 eV in $L1_2$ phase (Figure 6 (a)) disappeared in $D0_{22}$ ε_2 spectrum. There is a deep valley like structure observed at point C. The curve has one most prominent peak B at 1. 03eV, and a double peak feature A and A' (at 1.75 eV and 2.19 eV) after the deep valley like structure. Some small bumps are also present after the double peak feature. The curve ascends sharply as in case of $L1_2$ phase but at different energy value (below 0.70 eV). The curve is featureless above energy values of 6.50 eV as observed in $L1_2$ phase. To the best of our knowledge there are no experimental data to compare our calculated results with.

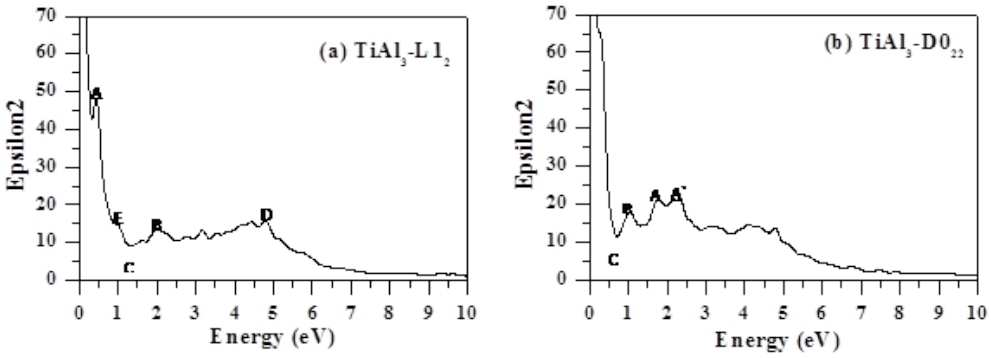

FIG. 6: Calculated imaginary part of the dielectric function of the two phases (a) $L1_2$ and (b) $D0_{22}$ of $TiAl_3$ intermetallic alloy system.

The interband optical conductivity (σ) is an important physical observable which can

be directly compared with experimental data. In the OLCAO approach, the real part of the optical conductivity is obtained by $\sigma = \frac{\varepsilon_2 \omega}{4\pi}$ after evaluating $\varepsilon_2(\omega)$ using relation 5 given in Section III. The optical conductivity spectrum for $L1_2$ phase using supercell approach is shown in Figure 7 (a). The spectrum has four prominent peaks A, B, C, and D at 0.47, 3.17, 4.44, and 4.80 eV respectively. Among these, peak D has largest amplitude and has a shoulder S on its right at 5.18 eV. The peaks B and C are prominent and wider appearing on the left of the main peak D. There are also some other small peak like features E, F, and G observed at 1.01, 2.04, and 5.74 eV respectively. The optical conductivity spectrum of $D0_{22}$ phase is shown in Figure 7 (b). The calculated σ shows three prominent peaks A, B, and C at 0.33, 2.34, and 4.77 eV respectively, and a double peak like feature DD' centered at 4.26 eV on the left of peak C. There is also a shoulder E present at 1.73 eV. A much deeper valley like region F exists at 0.67 eV. The highest peak D in $L1_2$ σ spectrum (Figure 7 (a)) seems to split in $D0_{22}$ phase. The part of σ spectra near the low energy end ($\sim$ 0 eV) shows a sharp increase in conductivity due to intraband transitions in metals. In this work intraband transitions are calculated using *ab intio* wave function, but usually approximated using Drude model ($\sigma(\omega) = (\sigma_o/1 + i\omega\tau)$), where τ is the relaxation time. We have also observed that interband transitions in $TiAl_3$ start at about 3.02 eV.

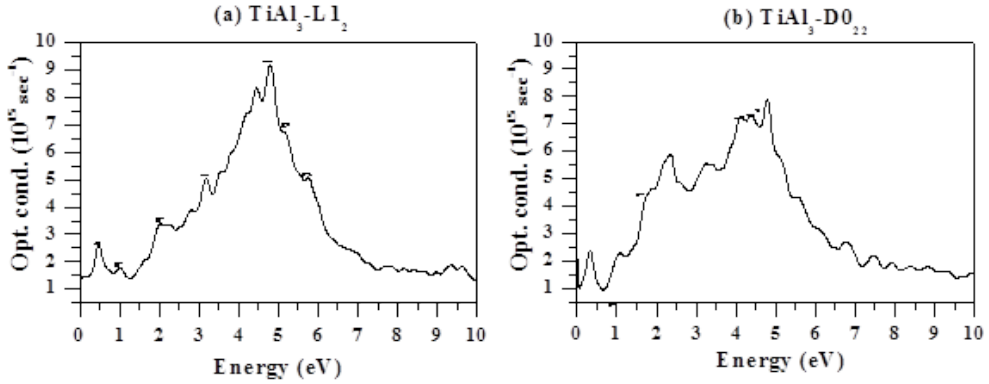

FIG. 7: Optical conductivity spectra of the two phases (a) $L1_2$ and (b) $D0_{22}$ of $TiAl_3$ intermetallic alloy system.

V. CONCLUDING REMARKS

In this study, we performed calculations on electronic structure, mechanical, and optical properties of $L1_2$ and $D0_{22}$ phases in $TiAl_3$ intermetallic alloy system. We used primitive as well as supercell approach in this work. Band structure calculations show that same number of bands cross the Fermi level ($E_F = 0$) in both the $L1_2$ and $D0_{22}$ phases.

Density of states calculations reveal that TDOS spectra of both the phases are dominated by Ti 3d-orbitals. However, the top of valence band is contributed mostly by the Al-2p states. The Fermi level cuts at the steeper side of the TDOS spectra in both phases. Larger number of states at the Fermi level exist in $D0_{22}$ phase 5.5 than $L1_2$ phase 4.67 states/(eV formula unit). Mulliken effective charge Q^* calculations show that more charge transfer ΔQ^* takes place in $D0_{22}$ phase than in $L1_2$ phase. This implies the behavior of $D0_{22}$ phase to be more ionic and stronger bonding and structure. Moreover the charge transfer trends in the two phases are quite opposite. In $L1_2$ phase, Ti atoms lose charge, while Al atoms gain the charge. On the other hand in $D0_{22}$ phase, Ti atoms gain charge and Al atoms lose. Localization index calculations provide the existence of highly localized states above the Fermi level within about 4 eV range in both the $L1_2$ and $D0_{22}$ phases.

Our calculated elastic stiffness constants reveal that there exists much diversity in the elastic behavior of the two $TiAl_3$ phases. All calculated C_{ij}'s for $L1_2$ phase are smaller than their corresponding values in $D0_{22}$ phase. This domination of the $D0_{22}$ phase seems to persist in the results on bulk mechanical properties (bulk modulus K, shear modulus G, and Young's modulus E) as well. The results on elastic stiffness constants and bulk properties are in good agreement with the measured data in literature. Optical conductivity spectra of the two phases although carry the most prominent peak structure at the same energy value of 4.80 eV nevertheless; the conductivity spectrum of $D0_{22}$ phase is not exactly the same as that of $L1_2$ phase.

Acknowledgments

Altaf Hussain is thankful to Prof. Dr. Wai-Yim Ching for his support and invitation to work with the Electronic Structure Group (ESG), Department of Physics and Astronomy, University of Missouri-Kansas City, Kansas City MO 64110, USA.

References

[1] V. K. Sikka, S. C. Deevi, and J. D. Vought, Adv. Mater. Process. **147**, 29 (1995).
[2] V. K. Sikka *et al.*, Intermetallics **12**, 837 (2004). doi: 10.1016/j.intermet.2004.02.034
[3] C. Colinet and A. Pasturel, J. Phys. Condens. Matter **14**, 6713 (2002). doi: 10.1088/0953-8984/14/26/311
[4] J. Braun and M. Ellner, Metallurgical and Materials Transactions **32**, 1037 (2001). doi: 10.1007/s11661-001-0114-x
[5] A. Hussain, S. S. Hayat, and M. A. Choudhry, Physica B **406**, 1961 (2011). doi: 10.1016/j.physb.2011.02.065
[6] R. Khoshhal, M. Soltanieh, and M. Mirjalili, Iran. J. of Mater. Sci. Engin. **7**, 24 (2010).
[7] Y. Q. Xie, Science in China E **41**, 146 (1998). doi: 10.1007/BF02919677
[8] Y. Q. Xie and X. D. Zhang, Science in China E **41**, 157 (1998). doi: 10.1007/BF02919678
[9] Y. Q. Xie, X. B. Liu, K. Peng, and H. J. Peng, Physica B **353**, 15 (2004).
[10] A. Hussain *et al.*, J. Alloys Comp. **509**, 5230 (2011). doi: 10.1016/j.jallcom.2011.02.071

[11] W. Li, G. Jianhong, and G. Jun, Adv. Mater. Res. **295-297**, 1305 (2011).
[12] W. Y. Ching, J. Am. Ceram. Soc. **73**, 3135 (1990). doi: 10.1111/j.1151-2916.1990.tb06430.x
[13] W. Y. Ching and P. Rulis, *Electronic Structure Methods for Complex Materials: The Orthogonalized Linear Combination of Atomic Orbitals*, Chap. 1–4, (Oxford University Press, Oxford, 2012).
[14] G. Kresse and J. Hafner, Phys. Rev. B **47**, 558 (1993). doi: 10.1103/PhysRevB.47.558
[15] G. Kresse and J. Furthmüller, Comput. Mater. Sci. **6**, 15 (1996). doi: 10.1016/0927-0256(96)00008-0
[16] W. Y. Ching, P. Rulis, L. Ouyang, and A. Misra, Appl. Phys. Lett. **94**, 051907 (2009). doi: 10.1063/1.3079800
[17] A. Hussain, S. Aryal, P. Rulis, M. A. Choudhry, and W. Y. Ching, Phys. Rev. B **78**, 195102 (2008). doi: 10.1103/PhysRevB.78.195102
[18] P. Hohenberg and W. Kohn, Phys. Rev. **136**, B864 (1964). doi: 10.1103/PhysRev.136.B864
[19] W. Kohn and L. J. Sham, Phys. Rev. **140**, A1133 (1965). doi: 10.1103/PhysRev.140.A1133
[20] S. Aryal, P. Rulis, and W. Y. Ching, Am. Mineral. **93**, 114 (2008). doi: 10.2138/am.2008.2664
[21] P. Rulis and W. Y. Ching, J. Mater. Sci. **46**, 4191 (2011). doi: 10.1007/s10853-011-5351-9
[22] C. C. Dharmawardhana, A. Misra, S. Aryal, P. Rulis, and W. Y. Ching, Cem. Concr. Res. **52**, 123 (2013).
[23] R. S. Mulliken, J. Chem. Phys. **23**, 1841 (1955). doi: 10.1063/1.1740589
[24] R. S. Mulliken, J. Chem. Phys. **23**, 1833 (1955). doi: 10.1063/1.1740588
[25] P. W. Anderson, Phys. Rev. **109**, 1492 (1958). doi: 10.1103/PhysRev.109.1492
[26] W. Voigt, *Lehrbuch der Kristallphysik*, (Teubner, Leipzig und Berlin, 1928).
[27] A. Reuss and Z. Angew., Math. Mech. **9**, 49 (1929). doi: 10.1002/zamm.19290090104
[28] R. Hill, Proc. Phys. Soc. A **65**, 349 (1952). doi: 10.1088/0370-1298/65/5/307
[29] A. Dwivedi and J. Bradley, *Mechanical response of titanium aluminide ($TiAl_3$)* (Army Research Laboratory 2010).
[30] M. Nakamura and K. Kimura, J. Mater. Sci. **26**, 2208 (1991). doi: 10.1007/BF00549190